Supplementary information: Steric effects in the adsorption of O_2 on a Cu(111) surface

Lok Yiu Wu,[a,b§] Maksymilian J. Roman,[a*]
Brianna R. Heazlewood,[a] and Mitsunori Kurahashi[c*]

*Corresponding authors: Maksymilian J. Roman, m.j.roman@liverpool.ac.uk;
Mitsunori Kurahashi, kurahashi.mitsunori@nims.go.jp

1 Molecular beam properties

The time-of-flight (ToF) profiles for the molecular beams used in this experiment are shown in Figure S1. The ToF profiles are obtained by measuring the arrival time of O_2 molecules at the quadrupole mass spectrometer (QMS), using the apparatus depicted in Figure 1 of the manuscript. The translational energy of the O_2 beam is varied by changing the ratio of O_2 and He carrier gas in the mixture. Table S1 sets out details of the gas mixtures, nozzle temperatures, incident energies (E_i), angles of incidence (θ_i), and normal incident energies (E_n) used in these measurements.

Table S1: Incident O_2 beam properties.

O_2:He ratio	Nozzle temperature (K)	E_i (meV)	θ_i (°)	E_n (meV)
10:2	298	87 ± 3	0	87 ± 3
			15	81 ± 3
			30	65 ± 2
5:12	298	150 ± 5	0	150 ± 2
			15	140 ± 5
5:12	298	154 ± 5	30	116 ± 4
			45	77 ± 2
4:21	298	212 ± 7	0	212 ± 7
			15	198 ± 6
			30	159 ± 5
			45	106 ± 3
5:82	298	313 ± 10	0	313 ± 10
			15	292 ± 9
			30	235 ± 8
			45	156 ± 5
5:76	468	421 ± 14	0	421 ± 14
			15	393 ± 13
5:76	468	423 ± 14	30	318 ± 10
			45	212 ± 7
2:38	573	548 ± 18	0	548 ± 18
			15	511 ± 17
			30	411 ± 13
			45	274 ± 9
			60	137 ± 4

[a] *Department of Physics, University of Liverpool, Oxford Street, Liverpool, L69 7ZE.*
[b] *Physical and Theoretical Chemistry Laboratory, University of Oxford, South Parks Road, Oxford, OX1 3QZ*
§ Current address: School of Chemistry, University of Birmingham, Edgbaston B15 2TT, United Kingdom
[c] *National Institute for Materials Science, 1-2-1 Sengen, Tsukuba, Ibaraki 305-0047, Japan*

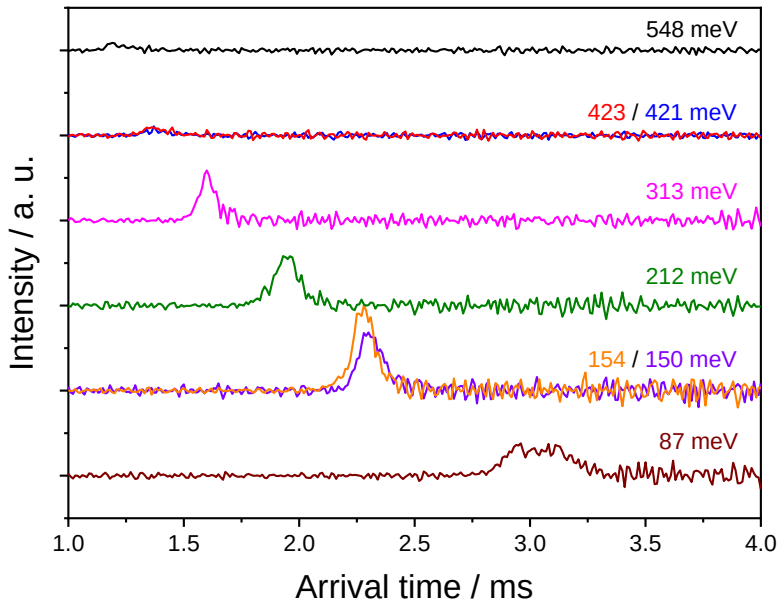

Figure S1: ToF profiles of the seeded O_2 molecular beams as measured by the QMS. Traces are coloured based on the incident energy of the beam (E_i), established from the position of the modal (peak) O_2 signal. Different energies are obtained by varying the O_2:He ratio and heating the nozzle (see Table S1). Beams produced under different conditions are offset in the y-axis for clarity.

2 Data analysis procedure

As described in the main text, while the magnetic field can be switched almost instantaneously to selectively align the O_2 molecules to either a helicopter or cartwheel geometry, the system does not respond to this change immediately. As such, only the data points taken after the system has completely adapted to the change can be used in the data analysis procedure. Three delays are chosen for the analysis of data recorded in each experimental run: d_1, the delay between the control and ion gauge signal for the first set of points in the first geometry; d_3, the delay between the control and ion gauge signal for the first set of points in the second geometry; and d_2, the delay for all the other points upon a change in magnetic field. An example is shown in Figure S2 for a helicopter versus cartwheel ([H *vs* C_z]) measurement. Data points are assigned to helicopter (a) or cartwheel (b) alignments, based on the magnetic field direction. The three delays defined above are shown on the figure. Points within these delays (in blue) are discarded, as they correspond to times when the system is still adapting to the change in magnetic field. All remaining data points (in orange) are retained for analysis.

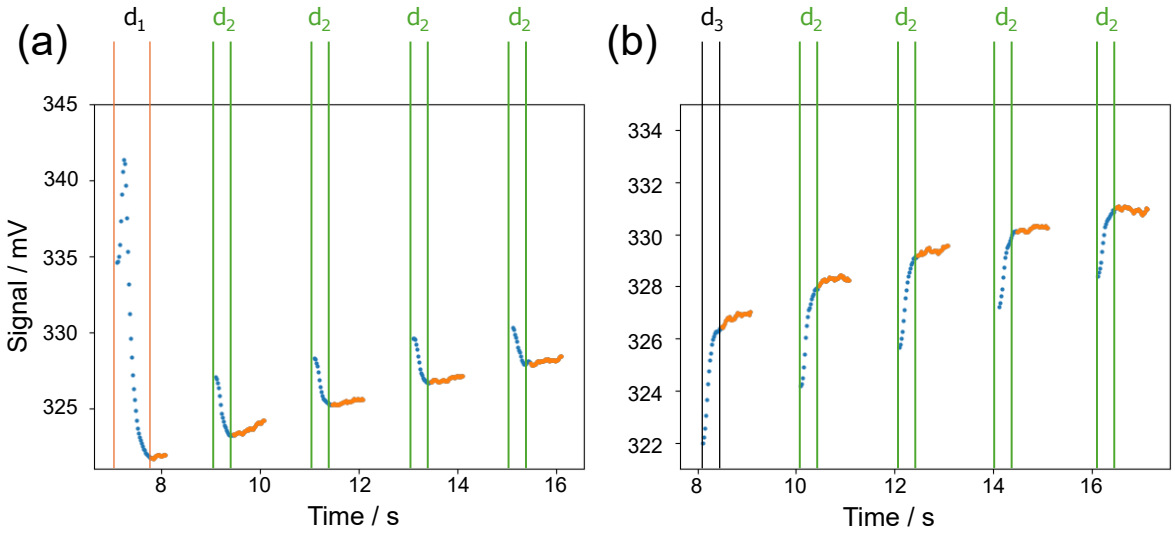

Figure S2: An illustration of the data selection procedure conducted prior to data analysis. The ion gauge signal is split into helicopter (a) and cartwheel (b) configurations, according to the control signal. Three delays, d_1, d_2, and d_3, are chosen, identifying regions where the conditions are not stable and where the data points are discarded. The remaining data points, shown in orange, are used in the data analysis procedure described in the main text.

3 Further experimental measurements

3.1 Additional helicopter versus cartwheel measurements

Additional King and Wells measurements conducted under different experimental conditions are provided. Figure S3 shows a comparison between the ion gauge signal collected at $\theta_i = 0°$, for a wide range of experimental incident energies (E_i = 87, 150, 212, 313, 421, and 548 meV). Figure S4 compares the data for E_i = 150 meV at angles of $\theta_i = 0°$, 15°, 30°, and 45°. Figure S5 shows the data recorded at a range of angles for E_i = 313 meV, and Figure S6 shows the same for E_i = 548 meV (with the addition of θ_i = 60°). Please refer to Figure 3 in the main text for a detailed description of the features of the data presented in Figures S3 to S5.

3.2 Cartwheel versus cartwheel measurements

Figure S7 shows a representative cartwheel(y) versus cartwheel(z) King and Wells measurement, conducted for $\theta_i = 0°$, covering a range of experimental incident energies (E_i = 87, 150, 212, 313, 421, and 548 meV). The data shows no steric effect between the two cartwheel alignments and this is true for measurements performed at all other experimental conditions considered here. We note that the measured $S_0(C_z)$ values from cartwheel versus cartwheel measurements are higher on average by about 12% relative to the equivalent $S_0(C_z)$ values obtained from helicopter versus cartwheel measurements collected as part of the same experimental run. For consistency, the $S_0(C_z)$ values obtained from the helicopter versus cartwheel measurements are used in Equations (1) and (3) in the analysis described in the main text.

3.3 Low surface temperature measurements

Trapping-mediated adsorption is facilitated by long interaction times between the surface and the adsorbate. Figure S8 shows the results of O_2 $S_0(\parallel)$ and $S_0(\perp)$ measurements performed at room temperature (*ca.* 300 K) and 107 K, conducted at low energies ($E_n < 150$ meV) and several angles of incidence. Lowering the surface temperature does not impact the sticking probability of O_2 on Cu(111) under the experimental conditions explored here; in all cases, the S_0 values measured at 107 K fall within the uncertainty ranges reported for the equivalent measurements performed at room temperature.

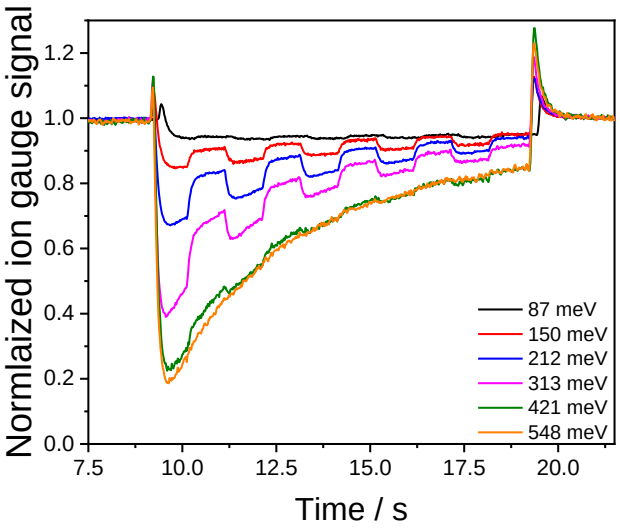

Figure S3: Helicopter versus cartwheel King and Wells measurements collected at $\theta_i = 0°$ and E_i = 87 meV (black), 150 meV (red), 212 meV (blue), 313 meV (magenta), 421 meV (green), and 548 meV (orange).

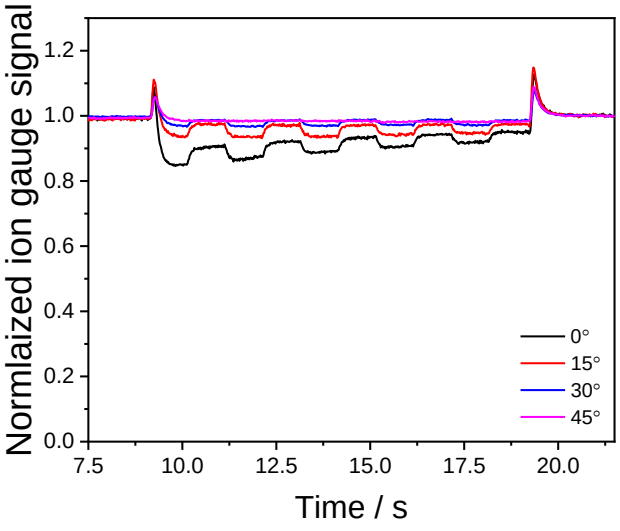

Figure S4: Helicopter versus cartwheel King and Wells measurements collected at E_i = 150 meV and incidence angles of $\theta_i = 0°$(black), 15°(red), 30°(blue), and 45°(magenta).

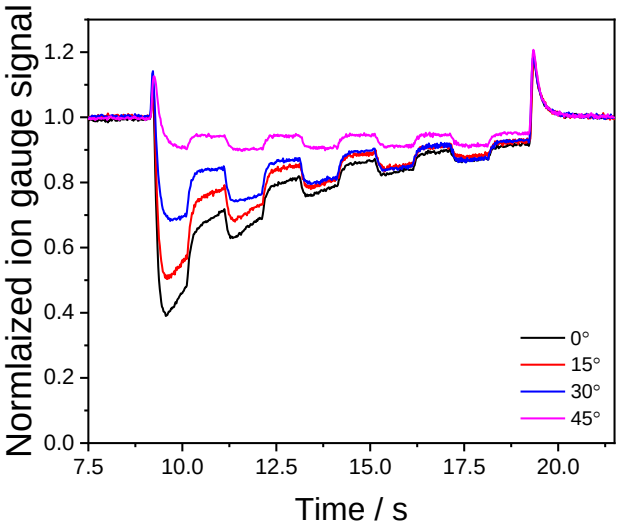

Figure S5: Helicopter versus cartwheel King and Wells measurements collected at $E_{\mathrm{i}} = 313$ meV and incidence angles of $\theta_{\mathrm{i}} = 0°$(black), 15°(red), 30°(blue), and 45°(magenta).

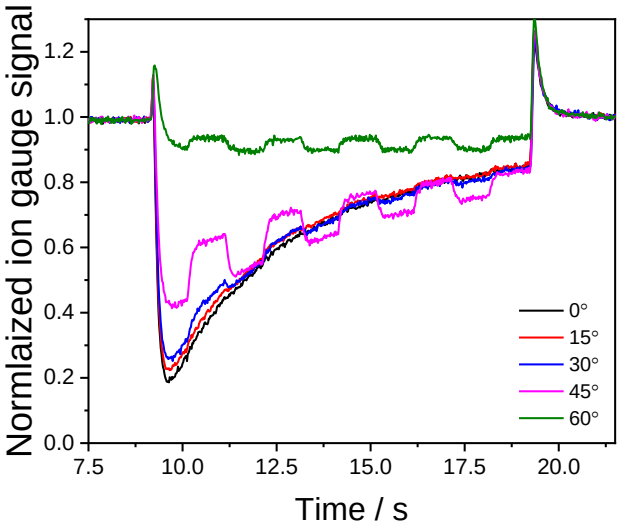

Figure S6: Helicopter versus cartwheel King and Wells measurements collected at $E_{\mathrm{i}} = 548$ meV and incidence angles of $\theta_{\mathrm{i}} = 0°$(black), 15°(red), 30°(blue), 45°(magenta), and 60°(green).

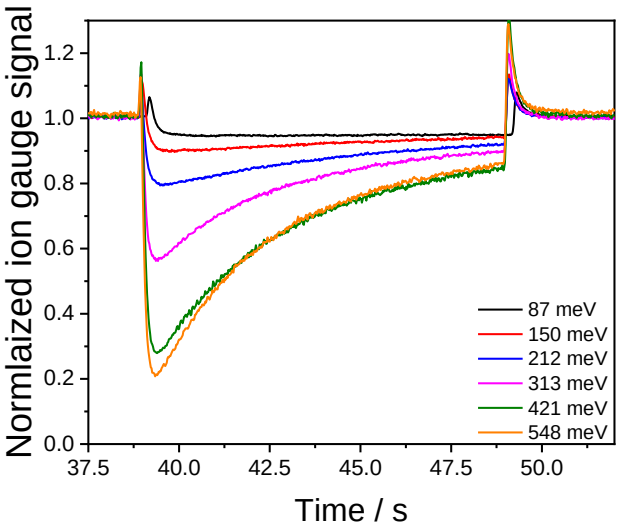

Figure S7: Cartwheel(y) versus cartwheel(z) King and Wells measurements collected at $\theta_i = 0°$ and E_i = 87 meV (black), 150 meV (red), 212 meV (blue), 313 meV (magenta), 421 meV (green), and 548 meV (orange).

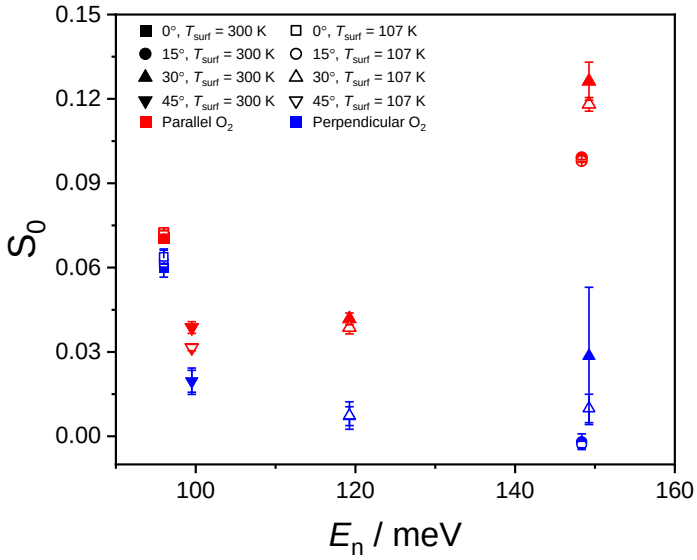

Figure S8: $S_0(\parallel)$ (red) and $S_0(\perp)$ (blue) values measured at 300 K (solid symbols) and 107 K (hollow symbols). Angles of incidence are denoted by the different symbol shapes.